Effect of CdSe/ZnS quantum dot dispersion on phase transitional behavior of 8OCB liquid crystal

Aysha Rani ●, Susanta Chakraborty ●, and Aloka Sinha ●*

Department of Physics, Indian Institute of Technology Delhi, Hauz Khas, New Delhi 110016, India

We report the effect on the phase transitional behavior of 8OCB liquid crystal (LC) doped with functionalized CdSe/ZnS quantum dots (QDs) in different concentrations. The temperature-dependent data of high-resolution optical birefringence and dielectric anisotropy are utilized to characterize the critical anomaly for both the isotropic-to-nematic (*I-N*) and nematic-to-smectic-*A* (*N*-Sm*A*) phase transitions. The obtained results reveal that the order parameter exponent (β) for the pure LC is found to be $\beta = 0.249$ and does not vary upon the inclusion of QDs in the pure matrix. It describes the weakly first-order characteristic of the *I-N* phase transition for all the studied samples, which falls within the limit of the tricritical hypothesis. Conversely, depending on the range of the *N* phase, we observed a nonuniversal nature of the specific heat capacity critical exponent (α') linked with the *N*-Sm*A* phase transition for all the studied samples. A relative comparison was made amongst the α' values extracted from both the anisotropy data, and further, a theoretical relationship is established with these exponent values. The coupling strength among the *N* and Sm*A* order parameters is determined using the optical birefringence data and discussed from the perspective of mutual interaction between the LC-QDs ligands. The results signify that a strong ligand-ligand interaction between neighboring QDs effectively reduces the *N* range and slightly influences the *N*-Sm*A* phase transition.

I. INTRODUCTION

Liquid crystals (LCs) form an intermediate thermodynamic state between the solid crystalline and isotropic liquid in the field of soft condensed matter. Over the last few decades, these anisotropic fluids have emerged as a suitable medium for the dispersion of nanoparticles (NPs) which has attracted broad interest in the research field due to numerous fascinating applications [1–3]. In general, the dispersion of NPs with a diameter of $< \sim 100$ nm can significantly alter the properties of the host LC material. Authors of several studies have demonstrated that the dispersion of various NPs in the LC system can improve or modify these physical characteristics as a function of the shape, size, and doping concentration of the NP [2,4–8]. The fundamental reason for the alteration of these properties is the interactions that take place at the molecular level between the NPs and mesogenic molecules.

Recent investigations have shown that the addition of NPs can locally affect the ordering of the LC molecules in both the nematic (*N*) and the smectic-*A* (Sm*A*) phases [9]. The main reason lies behind the surface-anchoring strength and interaction among dopant and LC materials. Sometimes the interaction between NPs can interplay to increase or decrease the phase transition temperature. The dispersion of spherical NPs can effectively dilute the host LC, which reduces the orientational ordering and thereby the isotropic-to-nematic (*I-N*) phase transition temperature [10]. Notably, authors of several reports have suggested that a strong interaction between NPs effectively improves the order parameter of the LC material, which in turn enhances the phase transition temperature. Such

fluctuations in order parameters and phase transition temperature strongly follow the doping level of NPs loaded in the LC system. NPs can moderately affect the pretransitional fluctuations in the dielectric data near the transitions of the *I-N* phase and other mesophases [11,12]. Adiabatic scanning calorimetry (ASC) reveals that *N*-Sm*A* phase transition temperature reduces with increasing NP concentration in the LC systems [13,14]. Despite many authors elucidating the impact of NPs on the nature of phase transition in thermotropic LCs [15–19], investigations related to the basic understanding of concentration dependence are still lacking.

Based on the strength and nature of order-parameter coupling, the transitional character of different LC mesophases and associated universality classes have been suitably studied by analyzing the critical phenomena at the phase transition [17,18]. The *I-N* phase transition has a weakly first-order character, described in terms of a small change in latent heat. The critical exponent values extracted near this transition agree with the tricritical hypothesis (TCH) [19]. On the other hand, the values of critical exponents for the *N*-Sm*A* transition obtained from theoretical investigations show some discrepancy with the experimental results, and the diverging nature remains unclear. A three-dimensional *XY* universality model is expected to be followed by the *N*-Sm*A* phase transition. At the same time, some experimental findings suggested a nonuniversal behavior [20]. It has been examined that a crossover exists from the second to the first order at the tricritical point, depending on the *N* range. Interestingly, the coupling between the order parameters and director fluctuations has a major impact on the *N*-Sm*A* phase transition such that a weak coupling (wide *N* range) reveals a second-order nature, whereas strong coupling (narrow *N* range) results in a weakly first-order transition [19]. In this regard, it is quite intriguing to investigate

*aloka@physics.iitd.ac.in

the nature of the mesophase transitions with a variation of doping concentration which may easily facilitate the understanding related to the molecular interaction with NPs.

To ascertain the phase transitional behavior, earlier studies involved different experimental methods such as high-resolution calorimetry, light scattering, high-resolution birefringence, and dielectric spectroscopy measurements [15,16,17,21]. Moreover, the order parameters of LCs are directly related to the anisotropic properties of the LC system. In earlier investigations on the binary mixtures of LCs, the consistency of the critical exponent values obtained from the high-resolution optical birefringence and dielectric measurements was revealed [22,23]. Thus, it is feasible to examine the phase transitional anomaly by using the same experimental techniques. In this paper, we aim to analyze the phase transitional behavior through the temperature-dependent optical and dielectric properties of LC nanocolloids by incorporating CdSe/ZnS quantum dots (QDs) at various concentrations in the 8OCB LC. The *I-N* phase transition is characterized by using the four-parameter power-law model from the temperature-dependent high-resolution optical birefringence data. Simultaneously, for the *N*-Sm*A* phase transition, both the optical and dielectric anisotropy measurements were used to calculate the corresponding critical exponents. The coupling effect between nematic-orientational and smectic-positional order near the *N*-Sm*A* phase transition is also discussed using the optical birefringence data by numerically fitting it with the analytical expression. These observations suggest that QDs can modify the strength of the coupling between nematic and smectic ordering, which is described in terms of different interaction mechanisms.

II. EXPERIMENT

To investigate the impact of QDs on the phase transitional property, we have chosen a dopant, surface-functionalized CdSe/ZnS QDs with an octadecylamine ligand (procured from Sigma-Aldrich, Merck, with diameter ∼5.6 nm). Three distinct mixtures were prepared by dispersing QDs in the host LC material, 4′-octyloxy-4-cyanobiphenyl (8OCB, Thermo Fisher Scientific) with concentrations of $x_{QDs} = 0.1, 0.2$, and 0.3 (in wt. %). The homogenous mixtures were prepared by dispersing QDs into chloroform and mixing the required volume concentration of QD solution with LC [24]. The resulting solutions are ultrasonicated using a digital ultrasonicator bath (Labman, Scientific Instruments Pvt. Ltd, India) for ∼1 h and 40 min until the optically homogenous mixture is achieved, finally heated at 60 °C on the hotplate for 1 h and left overnight at room temperature for the complete evaporation of the solvent [24]. These mixtures were further filled in commercially available indium-tin-oxide-coated homeotropic and planar-aligned cells (Instec Inc.) of different thicknesses (9 and 5 µm, respectively) to accomplish the experimental optical and dielectric study. The textures of the pure and doped samples were observed during cooling with a rate of 0.5 K/min from the isotropic state by using a polarizing optical microscope (OLYMPUS BX-51P, Tokyo, Japan) in the transmission mode with the planar-aligned LC cells placed between the crossed polarizer and analyzer. The uniformity of the recorded photomicrographs in the *N* and Sm*A* phases represents the
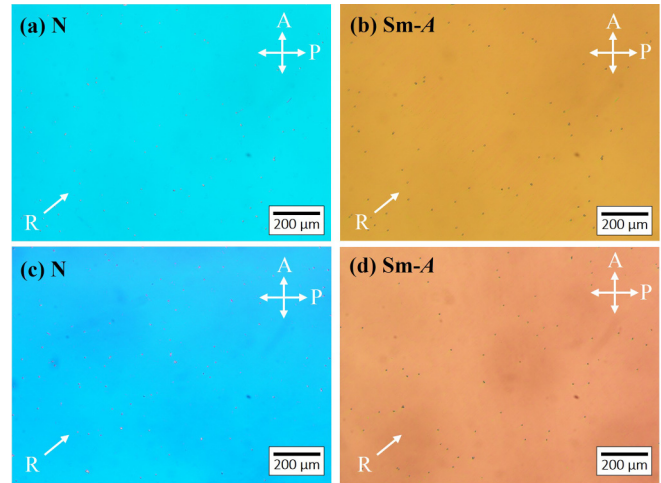

FIG. 1. Polarizing optical microscope images of the textures observed under crossed polarizers for the (a) and (b) pure and (c) and (d) $x_{QDs} = 0.1$ doped samples in the *N* (348 K) and Sm-*A* phases (331 K) during the cooling cycle measurement at a 0.5 K/min rate. Here, R denotes the rubbing direction 45° with respect to the crossed polarizers (indicated by A and P) and the scale bar is 200 µm.

homogenous alignment of the LC molecules along the rubbing direction, as shown in Fig. 1. No aggregation of QDs was noticed throughout the cell with time in all the doped samples, revealing the even distribution of QDs in the LC matrix. A slight change has been seen in the color of the textures for the $x_{QDs} = 0.1$ doped sample compared with the pure LC due to a small change in the birefringence of the sample. Similarly, in the other doped samples, a slight variation in color was found compared with the pure and $x_{QDs} = 0.1$ doped samples. The temperature-dependent high-resolution optical birefringence measurements were obtained by adopting a method described elsewhere [25]. A laser beam of wavelength $\lambda = 632$ nm transmits through the planar-aligned cells, placed between crossed Glan Thomson linear polarizers (Model-GTH10M, Thorlabs Inc.) such that the optic axis of LC molecules lies at 45° with either the polarizer or analyzer pass axis. The transmitted intensity was then detected by the assembly of S120C photodiode with a PM100D power meter (Thorlabs Inc.), and finally, the temperature-dependent intensity data were acquired via the MATLAB platform. In terms of phase retardation ($\Delta\varphi$), the normalized transmitted intensity can be expressed as

$$I_t = \frac{\sin^2 2\theta}{2}(1 - \cos\Delta\varphi), \tag{1}$$

where $\Delta\varphi = \frac{2\pi}{\lambda}d\,\Delta n$; λ is the wavelength of the incident light, d is the thickness of the LC cell, and θ is an angle equal to 45° made by the optic axis with the pass axis of the polarizer or analyzer. By analyzing $\Delta\varphi$ from the measured normalized intensity data, the temperature variation of Δn was evaluated for all the prepared samples. To assess the dielectric anisotropy data, temperature-dependent parallel and perpendicular static dielectric permittivity components ($\varepsilon'_\parallel$ and $\varepsilon'_\perp$) was acquired at a fixed 10 kHz frequency from the variation of capacitance of the planar and homeotropic cells, respectively. For these measurements, a test voltage of 0.1 V (less than the threshold
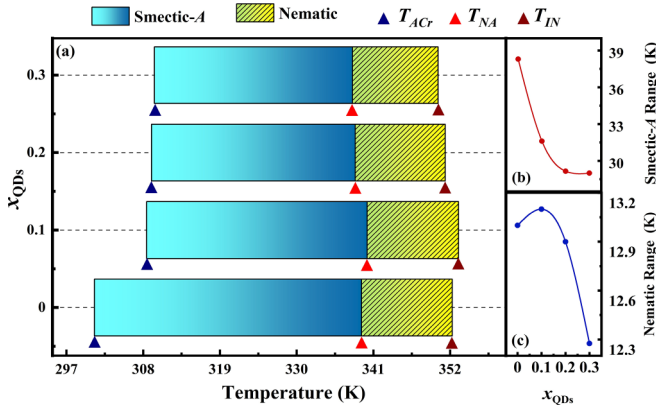
FIG. 2. (a) Phase diagram for the pure and quantum dots (QDs) doped 8OCB liquid crystal (LC) samples. Variation of (b) Sm*A* and (c) *N* ranges as a function of x_{QDs} loading in the pure sample.

FIG. 3. Temperature variation of Δn for the pure and quantum dots (QDs) doped liquid crystal (LC) samples filled in planar 5 μm cell thickness. Dashed lines portray the respective T_{NA} phase transition temperatures and the solid lines (in red) represent the fitted data with Eq. (2). The data were obtained at a cooling rate of 0.5 K/min.

voltage) was applied to the LC cells using a 20 Hz to 2 MHz Agilent E4980A precision LCR meter (Keysight Technologies) and data was obtained through the computer-controlled program. For both optical and dielectric studies, the temperature was controlled by placing the samples inside the hot stage (Model-HCS302, Instec Inc.) and regulated by a thermocontroller (Model-mk1000, Instec Inc.) having ±0.1 °C accuracy. Note that, prior to all measurements, pure and doped samples were heated up to 5 K above the nematic-to-isotropic phase transition temperature, and data were acquired with a cooling rate of 0.5 K/min.

III. RESULTS AND DISCUSSION

A. Phase diagram

The phase diagram for the pure 8OCB and the constituent mixtures with QDs is illustrated in Fig. 2. The associated mesophase transition temperatures: *I-N* (T_{IN}), *N*-Sm*A* (T_{NA}) and smectic-*A* to crystalline (T_{ACr}) are observed from the temperature-dependent Δn measurements. The transition temperatures T_{IN} and T_{NA} are slightly increased in the $x_{QDs} =$ 0.1 doped sample than the pure 8OCB host, changing from 352.3 to 353.2 K and 339.3 to 340.1 K, respectively. It is worth noting that the error in determining the phase transition temperature is limited within the ±0.02 K range. The increment in transition temperatures can be assumed due to the mutual interaction between the molecules and QDs, resulting in an enhancement of molecular ordering, which often increases the *N* range (T_{IN}-T_{NA}) [24]. Similar enhancements in transition temperatures were reported for 8OCB + graphene nanoplatelets, 8CB + $Sn_2P_2S_6$, and 5CB + TiO_2 doped systems [26–28]. Further increasing the doping concentration from 0.1 to 0.2, the values of T_{IN} and T_{NA} decreased by ∼1.26 and ∼1.35%, respectively, compared with the pure sample. The reduction in transition temperatures is more pronounced upon loading of higher QD concentration in the host system, and accordingly, the width of the *N* and smectic-*A* range (T_{NA}-T_{ACr}) decreases substantially in the $x_{QDs} = 0.3$ doped sample. In an earlier investigation, it was revealed that, to minimize the free energy contribution, the QDs can form an arrangement into groups which results in lowering the values
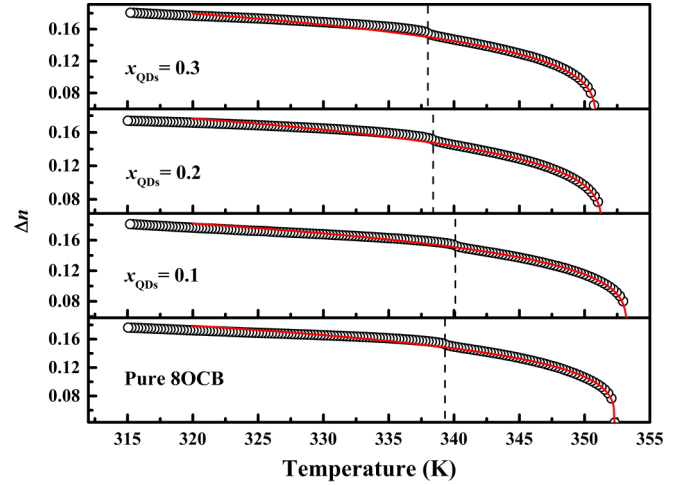
of T_{IN} and T_{NA} for $x_{QDs} > 0.65$ in the 8CB LC [9]. It suggests that the mutual interaction among the host molecules and dopant NPs likely changes the organization of QDs and mesogenic molecules, causing a reduction in transition temperatures. Also, it has been reported that the dispersion of ferroelectric NPs in the 8CB LC host can lower the value of T_{IN} compared with the pure sample due to the presence of free oleic acid molecules [29]. These free oleic acid ligands can effectively lower the ordering of the LC molecules and affect the physical attributes of the host LC system [30]. Thus, we speculate that, in the $x_{QDs} = 0.2$ and 0.3 doped samples, both the free ligands and interaction mechanism among QDs and mesogenic molecules affect the molecular ordering and contribute similarly to lower both the phase transition temperature. Moreover, the T_{ACr} value continues to rise with an increasing amount of QDs in the pure matrix from 301 to 309.6 K in the $x_{QDs} = 0.3$ doped sample, indicating that QDs act as nucleation sites for increasing the crystallization temperature.

B. Isotropic-to-nematic transition

The temperature variation of the optical birefringence $\Delta n(T)$ data is shown in Fig. 3 for the pure and QDs doped samples. To determine the reproducibility of the Δn behavior near the transition points, temperature-dependent measurements have been repeated multiple times, and close agreement has been found between the sequential datasets. All the mixtures, including the pure 8OCB sample, manifest a steep rise at the entrance of the *N* phase, attributable to the augmentation in the orientational order. As the temperature further reduces, the value of Δn exhibits a noticeable discontinuity at the transition region, owing to the growth of short-range smecticlike order near the transition, which consecutively strengthens the order parameter. Note that the Δn data for all the doped samples demonstrate a similar characteristic pattern with temperature.

TABLE I. Value of parameters evaluated from fitting the Δn data in the N phase with Eq. (2) and corresponding χ_v^2 value of the best fit for the pure 8OCB and QDs doped LC samples.

LC sample	T_{IN} (K)	ζ	S^{**}	T^{**} (K)	β	χ_v^2
Pure 8OCB	352.3	0.3003 ± 0.003	0.0989 ± 0.023	352.31 ± 0.154	0.2494 ± 0.013	1.011
$x_{QDs} = 0.1$	353.2	0.3025 ± 0.003	0.1013 ± 0.005	353.22 ± 0.019	0.2483 ± 0.006	1.010
$x_{QDs} = 0.2$	351.3	0.2980 ± 0.002	0.1003 ± 0.004	351.32 ± 0.020	0.2494 ± 0.004	1.011
$x_{QDs} = 0.3$	350.7	0.3047 ± 0.011	0.0995 ± 0.010	350.85 ± 0.037	0.2505 ± 0.014	1.020

According to the model developed by Vuks [31] and Chandrasekhar and Madhusudana [32], the orientational order parameter S is directly linked with Δn. The temperature variation of S can be determined with the four-parameter power-law equation, compatible with the mean-field theory, which describes the weakly first-order transition for both the critical and tricritical behavior [33]. It relates the temperature behavior of Δn in the following form [34]:

$$\Delta n(T) = \zeta \left[S^{**} + (1 - S^{**}) \left| \frac{T - T^{**}}{T^{**}} \right|^\beta \right], \qquad (2)$$

where $\zeta = (\frac{\Delta \alpha}{\alpha})[\frac{n_I^2 - 1}{2n_I}]$, n_I is the refractive index value in the I state pointing immediately higher to T_{IN}, α is the molecular polarizability, and $\Delta \alpha = \alpha_l - \alpha_t$ is the molecular polarizability anisotropy with α_t being the transverse (perpendicular) and α_l is the longitudinal (parallel) polarizability relating to the long axis of the molecule. Here, T^{**} is the effective second-order transition temperature, S^{**} is the value of S at $T = T^{**}$, and β is the order parameter critical exponent. The above equation consists of the four parameters (ζ, S^{**}, T^{**}, and β) and is utilized to analyze the impact of doping on the character of the I-N transition by fitting the $\Delta n(T)$ data for all the investigated samples. The fitting process is carried out by using the Leverberg-Marquardt algorithm using the nonlinear curve fitting tool in Origin software. During the fitting procedure, data points at each extreme of the N range were discarded to avoid both the nematic-isotropic coexistence region and the pretransitional fluctuation of the SmA phase. This double-range shrinking technique allows 10 K of the data range in the N phase for the fitting purpose. Subsequently, the reduced error function χ_v^2 defined in Eq. (3) [35] is computed (using the MATLAB program) to check the quality of the fits:

$$\chi_v^2 = \frac{\frac{1}{\nu} \sum_i (y_i - f_i)^2}{\sigma^2}, \qquad (3)$$

where f_i is the ith fit value analogous to the y_i measured value, $\nu = N - p$ is the degrees of freedom with N being the total number of data points, p is the number of fitting parameters, and σ^2 is the variance of the experimental data. The value of χ_v^2 falling in the range between 1 to 1.5 represents a good fit [35]. The corresponding fitted curves to Eq. (2) are shown in Fig. 3, which is extrapolated to the SmA region, and the fitted parameters are tabulated in Table I. It is observed that the average value of β is 0.249 ± 0.008 for all the doped samples and close to the value obtained for the 8OCB host. This value is found to be consistent with the TCH, as primarily predicted by Keyes [36] and Anisimov *et al.* [37,38] for the I-N transition. Therefore, the addition of QDs does not affect the nature of the I-N transition and follows a weakly

first-order character for all the studied samples. Similar behavior has been reported for several LC mixtures [20,34] as well as nanodoped LC systems, such as 8OCB + ZnS [17], 8CB + CdSe [39], and 8CB + multiwalled carbon nanotubes [19] from the high-resolution birefringence studies. Additionally, we can observe from Table I that the value of T^{**} is found to be slightly higher than T_{IN} for all the samples, and the magnitude of ζ and S^{**} parameters do not vary significantly by the QD doping in the 8OCB LC system.

C. Nematic-to-smectic-A transition

It is anticipated that, with the advent of smectic layering, the orientational ordering will enhance in the LC systems. This augmentation is determined by the coupling strength among the SmA and N order parameters [33,39]. For this coupling, de Gennes [40] has postulated a relationship $S - S_0 = C \chi \langle |\Psi| \rangle^2$ in accordance with the mean-field model, where $|\Psi|$ is the SmA order parameter, C is the coupling constant, χ is a response function, and S_0 is the value of the N order parameter without any smectic ordering. By considering the influence of fluctuations in the order parameters and short-range smectic ordering, the earlier described relation can be rewritten into the following form [41]: $S - S_0 \sim \langle |\Psi|^2 \rangle$. Further, a relation for the temperature behavior of $\langle |\Psi|^2 \rangle$ can be established as a result of the Landau–de Gennes free energy model [42,43], which is given as

$$\langle |\Psi|^2 \rangle = A + B_\pm \left| \frac{T - T_{NA}}{T_{NA}} \right|^\lambda, \qquad (4)$$

where T_{NA} represents the N-SmA transition temperature, subscript $\pm$ relates to quantities above (+) and below (−) T_{NA}, and $\lambda = 1 - \alpha$, signifying the limiting behavior of the N order parameter with α being the specific heat capacity critical exponent. The validity of the above equation was thoroughly tested for the n-alkyl cyanobiphenyl and n-alkyloxy cyanobiphenyl homologous series through the high-resolution Δn data [39].

Although the theoretical predictions for the N-SmA phase transition suggest that it belongs to the three-dimensional XY (3D-XY) universality class [44], many experimental investigations have failed to provide a clear image of this universality class [45,46] as a reason for the coupling between the N director fluctuations and order parameters. Based on the coupling strength between S and $|\Psi|$ or by the N range, there exists a tricritical point through which the nature of the N-SmA phase transition changes from the second- to the first-order character [46,47]. It is referred to as the second order for a broad N range (i.e., for weak coupling) and becomes the first order for a narrow N range (i.e., for strong coupling).
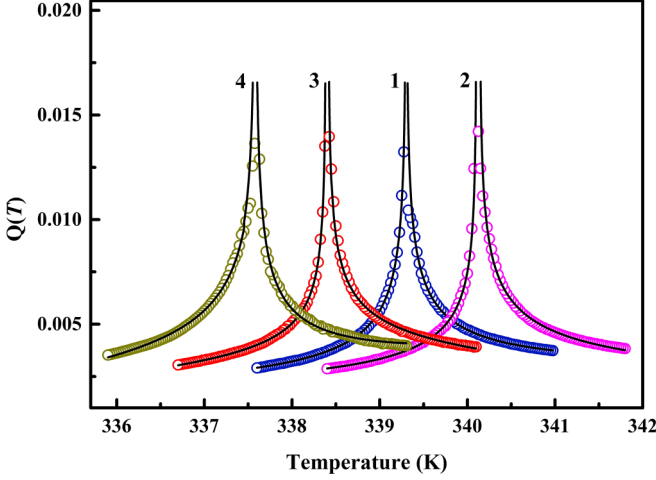
FIG. 4. Temperature dependence of the quotient $Q(T)$ in the neighborhood of the N-SmA phase transition for the pure and doped liquid crystal (LC) samples. Curve 1: $x_{QDs} = 0$ (pure), Curve 2: $x_{QDs} = 0.1$, Curve 3: $x_{QDs} = 0.2$, and Curve 4: $x_{QDs} = 0.3$ are shown in the figure for all the studied samples. The solid line (in black) indicates the fitting of the data with Eq. (6). Curve 4 has been shifted toward the left side by 4 K for a better representation.

To obtain better insight into the coupling strength between the N and SmA order parameters, we analyzed the phase transitional anomaly using the Δn and anisotropy data of dielectric permittivity in this section. As evident from Fig. 3, the N-SmA phase transition seems to be continuous, and no visible discontinuity is observed at T_{NA}. A first-order temperature derivative of Δn (i.e., $n' = -d(\Delta n)/dT$) provides an extremum point which can be regarded as the estimated phase transition temperature [17]. This quantity n' is found to be linked to the anomaly of the specific heat capacity and can be used to explore the critical behavior related to the transition [17,48]. However, a slight temperature gap between the two successively recorded measuring points causes the analytically computed n' to produce scattered points, making it unsuitable for the current investigation. Thus, it is plausible to exploit a differential quotient $Q(T)$, which is expressed as [17,19,46,49]

$$Q(T) = -\frac{\Delta n(T) - \Delta n(T_{NA})}{T - T_{NA}}, \quad (5)$$

where $\Delta n(T_{NA})$ represents the value of Δn at T_{NA} transition temperature. The quotient $Q(T)$ is identical to $C(T) = -[H(T) - H_c]/[T - T_c]$, where $H(T)$ accounts for temperature-dependent enthalpy realized from the ASC data [50]. Like the quotient $C(T)$, the quantity $Q(T)$ follows the same power-law divergence behavior with a similar exponent

α' comparable with the α value [46]. To quantify the limiting behavior of $Q(T)$, the measured $Q(T)$ data near the N-SmA phase transition [51,52] have been fitted to:

$$Q(T) = A^{\pm}\tau^{-\alpha'}(1 + D^{\pm}\tau^{\Delta}) + \frac{C(T - T_{NA})}{T_{NA}} + B, \quad (6)$$

where $A^{\pm}$ are the critical amplitudes higher (+) and lower (−) than T_{NA}, the reduced temperature $\tau = |(T - T_{NA})/T_{NA}|$, α' is the critical exponent analogous to α, $D^{\pm}$ are the coefficients of first corrections-to-scaling terms, Δ is the first corrections-to-scaling exponent, $C(T - T_{NA})/T_{NA}$ symbolizes the temperature-dependent part of the regular background contribution, and B denotes the combined regular and critical background term. For the 3D-XY case, the value of Δ is taken as 0.524, and in this paper, it is kept at 0.5 [53]. The $Q(T)$ data of all the samples have been fitted to Eq. (6) within the range of $|\tau| = 5 \times 10^{-3}$, as depicted in Fig. 4, with a procedure described above and keeping T_{NA} as fixed. It should be emphasized that like the work reported by Zywociński *et al.* [54], we noticed that multiplying C by $(T - T_{NA})/T_{NA}$ instead of $(T - T_{NA})$ in the above equation has suppressed the temperature fluctuations and associated background contribution from the experimental data, which improves the quality of the fit. The fit to Eq. (6) is shown graphically in Fig. 4 by solid lines on each side of the N-SmA phase transition, and related values of the fitted parameters are listed in Table II. To reduce the error caused by experimental uncertainty, a few data points near T_{NA} were omitted during the fitting process. Likewise, the χ_v^2 parameter, given in Eq. (3), is used to affirm the fit quality and shows a maximum value of ~1.049 among all the investigated samples. It is worth mentioning that the fitting range is selected based on the minimum value of the reduced error function χ_v^2. As detailed in the figure, the $Q(T)$ curve shows a sharp peak in the vicinity of T_{NA} for all the investigated samples. The value of α' is found to be comparable above and below the phase transition for all the studied compounds, and for simplicity, an average value has been presented in the table. For the pure 8OCB LC, $\alpha' = 0.2003 \pm 0.0015$, which is in line with the values reported in the literature from the high-resolution Δn measurements [17,34]. By incorporating QDs into the pure system, the value of α' first decreases for the sample $x_{QDs} = 0.1$ and then increases linearly with increasing QDs concentration from 0.1899 ± 0.073 for $x_{QDs} = 0.1$ to 0.21 ± 0.0004 for the $x_{QDs} = 0.3$ doped sample. This non-monotonous behavior of α' follows an inverse variation of the N range with x_{QDs}, as indicated in Fig. 2. A decrement in the value of the N range for the heavily doped ($x_{QDs} = 0.2$ and 0.3) samples clearly outlines the strengthening of the coupling between the nematic-orientational and smectic-positional ordering. It might be possible because of the mutual

TABLE II. Value of parameters evaluated from the fits of $Q(T)$ data to Eq. (6) and associated χ_v^2 value.

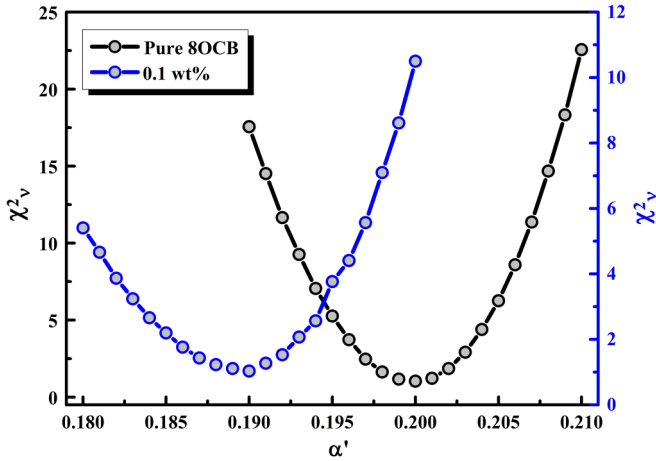| LC sample	T_{NA} (K)	α'	A^-/A^+	D^-/D^+	χ_v^2
Pure 8OCB	339.3	0.2003 ± 0.001	1.0146 ± 0.022	1.0050 ± 0.032	1.049
$x_{QDs} = 0.1$	340.1	0.1899 ± 0.073	0.8961 ± 0.071	1.1240 ± 0.137	1.048
$x_{QDs} = 0.2$	338.4	0.2079 ± 0.008	0.9216 ± 0.077	1.0351 ± 0.090	1.046
$x_{QDs} = 0.3$	338.0	0.2100 ± 0.001	1.0256 ± 0.104	0.8592 ± 0.110	1.048

FIG. 5. Variation of χ_v^2 achieved from the fits of $Q(T)$ data by varying the critical exponent α' for the pure 8OCB and $x_{QDs} = 0.1$ doped liquid crystal (LC) samples.

interaction among mesogenic molecules and QDs. The estimated values of α' depict a nonuniversal type in nature in between those obtained for the 3D-XY ($\alpha = -0.007$) and TCH ($\alpha = 0.5$) cases [13]. In addition, for the pure 8OCB LC system, the ASC data yield an average value of $\alpha = 0.20 \pm 0.05$ near the N-SmA phase transition [21]. This value is quite consistent with the α' value attained from the $Q(T)$ data. Additionally, the McMillan ratio (R_M), which is defined as the ratio of T_{NA} to T_{IN} temperature can determine whether the N-SmA phase transition is first or second order with the presence of tricritical points. The value of R_M much closer to unity signifies a weakly first-order transition, and the tricritical point is characterized by a theoretical limit of $R_M = 0.87$ [21,55]. Nonetheless, some experimental investigations yielded a range of nonuniversal values from $R_M = 0.942$ to 0.995 [55]. In this paper, the values of R_M for both the pure and doped LC samples lie around 0.963, i.e., within the range of nonuniversal values, representing a second-order

nature of the N-SmA phase transition. We must stress that, for all the studied samples, the ratios of A^-/A^+ and D^-/D^+ are ~1, corroborating the symmetry in the $Q(T)$ wings above and below the T_{NA}. In an attempt to verify the correctness of the evaluated values of α' from the fits of $Q(T)$ data, the value of χ_v^2 has been determined using Eq. (3) as a function of the critical exponent values for all the samples. Figure 5 displays the χ_v^2 profile with varying α' values for the pure and $x_{QDs} = 0.1$ doped samples. The values of χ_v^2 for these profiles were obtained by fitting the $Q(T)$ data independently above and below T_{NA} against the variation of α' in a step of 0.001 while considering C and B as free parameters during the fitting procedure. As seen from the figure, the minima of the correspondent curve adequately reflect the value of α' as pointed out in Table II. For example, the minimal value of the χ_v^2 profile of the pure LC gives $\alpha' = 0.20$, uniform with the tabulated value as $\alpha' = 0.2003$. An equivalent pattern of the reduced error function vs the critical exponent has been demonstrated for a nonpolar smectogen LC compound by employing the temperature-dependent high-resolution Δn data near T_{NA} [33].

Like optical anisotropy, the temperature variation of dielectric anisotropy can also be related to the order parameter of the LC systems and consequently can be used to elucidate the phase transitional behavior associated with the transition. The dielectric anisotropy ($\Delta\varepsilon' = \varepsilon'_\parallel - \varepsilon'_\perp$) is the measure of the strength of the interaction between mesogenic molecules in response to the applied electric field. A representative plot of the temperature dependence of dielectric parameters ($\varepsilon'_\parallel$, $\varepsilon'_\perp$, $\Delta\varepsilon'$) for the pure 8OCB and $x_{QDs} = 0.1$ doped samples are presented in Fig. 6. Here, the value of average dielectric permittivity (ε_{avg}) is calculated as $\varepsilon_{avg} = \frac{1}{3}(2\varepsilon'_\perp + \varepsilon'_\parallel)$, and ε_{iso} represents the dielectric permittivity in the isotropic state. It is clear from the figure that all the dielectric parameters ($\varepsilon'_\parallel$, $\varepsilon'_\perp$, $\Delta\varepsilon'$) show a dramatic change from the I-N phase due to the enhancement of the orientational ordering. Nevertheless, a finite change in the values of all parameters has been noticed near T_{NA} because of the evolution of smecticlike short-range
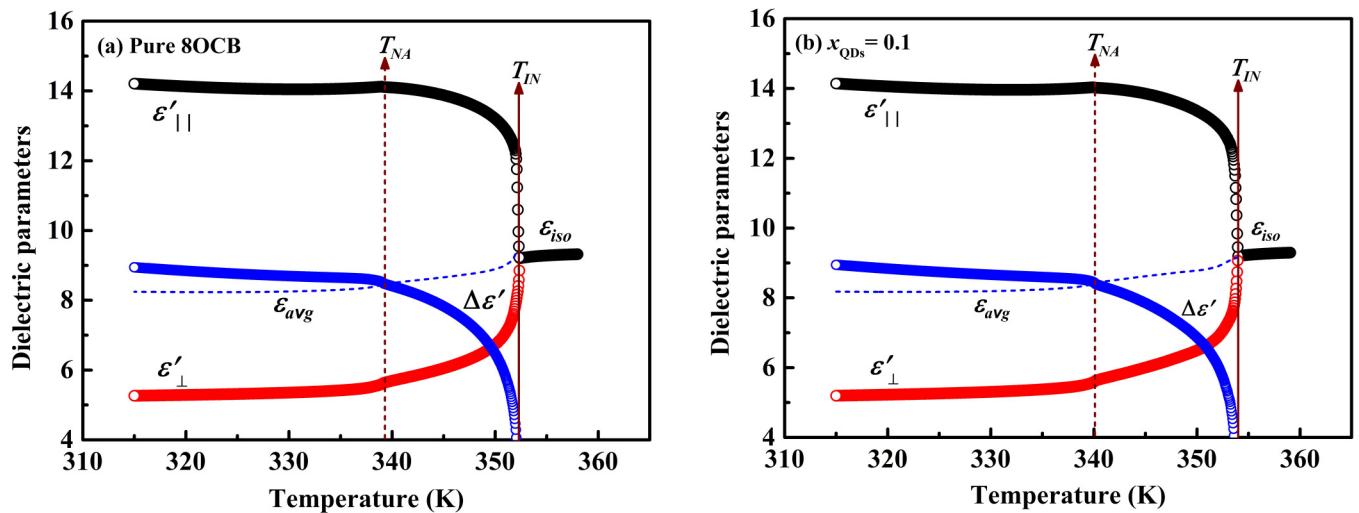

FIG. 6. Temperature dependence of dielectric parameters for the (a) pure 8OCB and (b) $x_{QDs} = 0.1$ doped liquid crystal (LC) samples filled in planar and homeotropic cells with 5 and 9 μm cell thickness, respectively. Solid and dashed arrows designate the T_{IN} and T_{NA} temperatures, respectively. The data were obtained at a cooling rate of 0.5 K/min.
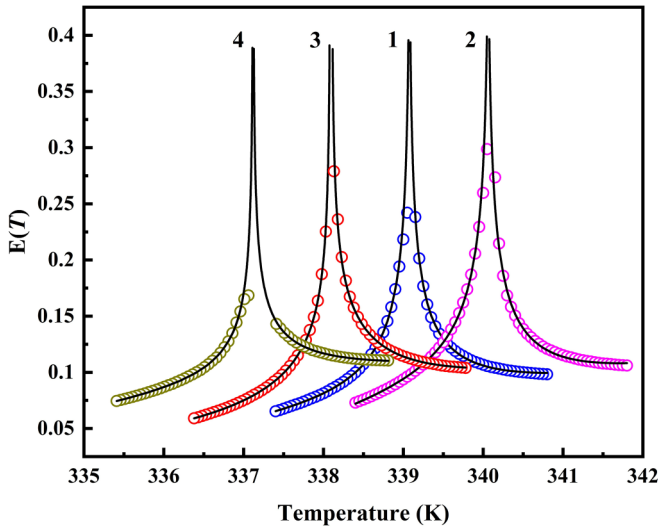
FIG. 7. Temperature dependence of the quotient $E(T)$ near the N-SmA transition for the pure and quantum dots (QDs) doped liquid crystal (LC) samples. The fitting of the data with Eq. (8) is represented by a solid line (in black). Curve 1: $x_{QDs} = 0$ (pure), Curve 2: $x_{QDs} = 0.1$, Curve 3: $x_{QDs} = 0.2$, and Curve 4: $x_{QDs} = 0.3$ are illustrated in the figure for all the studied samples. Curves 3 and 4 have been shifted toward the left side by 0.32 and 0.89 K, respectively, for a better representation.

ordering in the N phase. The value of $\varepsilon'_{\parallel}$ increases slowly, and that of $\varepsilon'_{\perp}$ shows a continual decrement upon reducing the temperature in the SmA phase, causing a net increment in the $\Delta\varepsilon'$ values. Thereby, both the pure and $x_{QDs} = 0.1$ samples exhibit positive values of $\Delta\varepsilon'$ throughout the mesomorphic region. The value of ε_{avg} is identified to be lower than the extrapolated value of ε_{iso} in the N and SmA mesophases on account of increased intermolecular interactions in both mesophases compared with the I state. All the dielectric parameters showed a similar characteristic profile in the other doped samples as well. Recently, researchers have examined that the dispersion of BaTiO$_3$ NPs (diameter of 50 nm) in calamitic LC compounds significantly influences the pretransitional fluctuations near the N-SmA transition [11,56,57]. Comparatively, QDs are smaller in size and surface functionalized with octadecylamine ligands that can affect the ordering of mesogenic molecules through the guest-host interaction mechanism [24]. Thus, to comprehend the effect of QDs on the N-SmA phase transitional character, it is imperative to evaluate the critical exponents in proximity to T_{NA} using $\Delta\varepsilon'(T)$ data for all the samples.

As one can see from Fig. 6, the $\Delta\varepsilon'(T)$ curve, like that of $\Delta n(T)$, shows no pronounced discontinuity at T_{NA}. Henceforth, a differential quotient $E(T)$ equivalent to $Q(T)$ can be defined by using $\Delta\varepsilon'(T)$ to quantify the critical exponent near T_{NA} in the following form [22], where $\Delta\varepsilon'(T_{NA})$ is the value of $\Delta\varepsilon'$ at T_{NA} transition temperature:

$$E(T) = -\frac{\Delta\varepsilon'(T) - \Delta\varepsilon'(T_{NA})}{T - T_{NA}}. \qquad (7)$$

Accordingly, the limiting behavior of $E(T)$ is characterized by the power-law expression, as given by Eq. (8) [22]:

$$E(T) = A^{\pm}\tau^{-\alpha'}(1 + D^{\pm}\tau^{\Delta}) + \frac{C(T - T_{NA})}{T_{NA}} + B. \qquad (8)$$

Here, α' is the critical exponent identical to α, and all the other parameters have their conventional meanings, as mentioned earlier concerning Eq. (6). Figure 7 illustrates the fitting of the $E(T)$ data for all the samples with Eq. (8), and Table III presents the resulting fitted parameters along with χ_v^2 values. It can be noted that the fitting was done within the same temperature range by setting $|\tau| = 5 \times 10^{-3}$ and by keeping Δ at a constant value of 0.5. A few data points on the SmA side of the $E(T)$ curve show deviated behavior, which has been eliminated during fitting. Figure 7 reveals that all the curves exhibit a sharp peak of almost the same height around T_{NA}, as seen in Fig. 4. Note that the value of α' in Table III (averaged values acquired from fitting above and below the N-SmA phase transition) coincides well with those measured from the fits of $Q(T)$ data for all the samples with an acceptable χ_v^2 value from 1.107 to 1.125. Again, the values of α' lie in between the 3D-XY ($\alpha = -0.007$) and TCH ($\alpha = 0.5$) limits, indicating the nonuniversal character of α' values. Therefore, equivalent to $Q(T)$ data, the quotient $E(T)$ expresses a power-law behavior with the similar α' values. Moreover, the ratios A^-/A^+ and D^-/D^+ for all the samples were observed to be close to unity, like those referred to in Table II. It implies that the $E(T)$ wings on the SmA and N sides possess symmetry, as do the $Q(T)$ wings [20]. To closely inspect the effectiveness of the obtained values of α' from the fits of $E(T)$ data, the χ_v^2 values as a function of the α' value for the pure and $x_{QDs} = 0.1$ doped samples are graphically shown in Fig. 8. By taking C and B as free parameters with T_{NA} as a fixed variable in Eq. (8), the χ_v^2 profiles are generated against the variation of the α' value in a step of 0.001. It is visible that the minimum of each curve is in reasonable agreement with the estimated values of α' from the $E(T)$ fitting function. All the other doped samples show a typical χ_v^2 profile whose minima correspond well with the distinctive α' values. It is worth concluding that, apart from high-resolution Δn data, $\Delta\varepsilon'$ measurements also convey

TABLE III. Value of parameters extracted by fitting the $E(T)$ data for the pure and doped samples to Eq. (8) near the N-SmA phase transition and related χ_v^2 value.

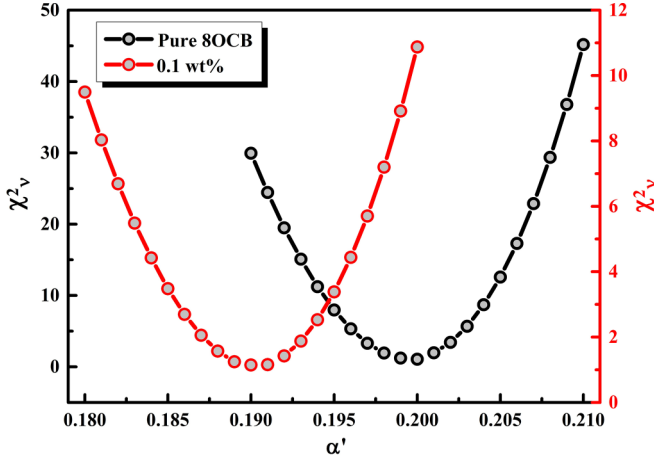| LC sample	α'	A^-/A^+	D^-/D^+	χ_v^2
Pure 8OCB	0.2002 ± 0.001	0.9913 ± 0.039	0.9638 ± 0.043	1.107
$x_{QDs} = 0.1$	0.1899 ± 0.007	0.9439 ± 0.168	0.9503 ± 0.084	1.107
$x_{QDs} = 0.2$	0.2075 ± 0.001	0.9465 ± 0.034	0.9795 ± 0.137	1.115
$x_{QDs} = 0.3$	0.2150 ± 0.003	0.9678 ± 0.063	1.0126 ± 0.067	1.125

FIG. 8. Variation of χ_v^2 generated from the fits of $E(T)$ data by varying the critical exponent α' for the pure 8OCB and $x_{QDs} = 0.1$ doped liquid crystal (LC) samples.

FIG. 9. Variation of Δn with temperature for the $x_{QDs} = 0.1$ doped sample. A solid line (in red) shows the fitting of the data above and below T_{NA} with Eq. (9). A vertical double-sided arrow in the inset indicates a change in the value of Δn at T_{NA}.

similar phase transitional behavior near T_{NA} in all the studied samples.

To further ascertain the effect of QDs doping on the coupling efficiency between the nematic and smectic-A order parameters, the $\Delta n(T)$ data close to the N-SmA transition are utilized to determine the value of the parameter λ, indicating the limiting behavior of the N order parameter. To test the validity of a theoretically predicted relation $\lambda = 1-\alpha$, the $\Delta n(T)$ data have been fitted above and below T_{NA} using the following expression [33]:

$$\Delta n(T) = \begin{cases} A_+|\tau|^{1-z}(1 + D_+|\tau|^{\Delta}) + B_+|\tau| + C_+ \\ A_-|\tau|^{1-z'}(1 + D_-|\tau|^{\Delta}) + B_-|\tau| + C_- \end{cases}, \quad (9)$$

where $\tau = |(T - T_{NA})/T_{NA}|$, the subscripts $(+)$ and $(-)$ denote above and below the T_{NA} temperature ranges, A is a constant, $B|\tau|$ is the temperature-dependent contribution of the regular background term, D is the coefficient of first corrections-to-scaling terms, and C represents a combined regular and critical background term. The transition temperature T_{NA} was determined from the individual fits to Eq. (9) by initially putting the values as obtained from the quantity $n' = -d(\Delta n)/dT$ and then setting it as a free parameter. The optimal value of T_{NA} was chosen from the minimum value of χ_v^2 obtained for fits above and below the transition temperature and by following the condition $z = z'$. A
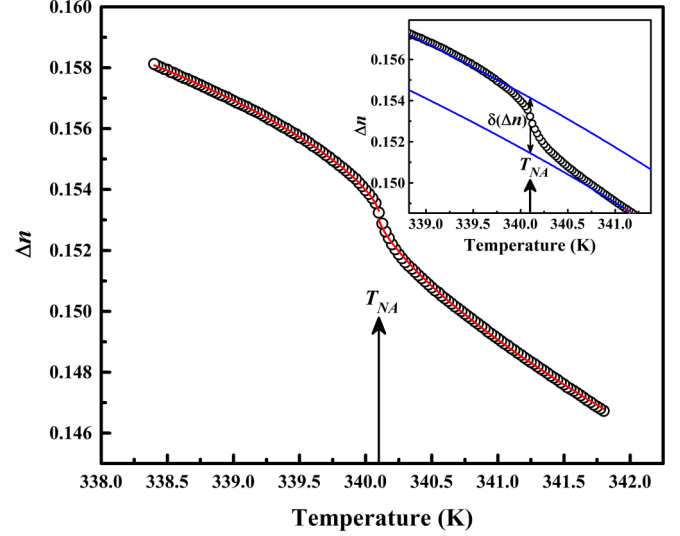
difference of $\sim\pm 2$ mK has been noticed in the value of T_{NA} for all the samples as compared with that observed from the quantity n'. Notably, after including the correction terms, $D_+ \neq D_- \neq 0$ into the above expression does not make any substantial improvement in the fit quality. Therefore, we set the constraint $D_+ = D_- = 0$, which follows those reported in Refs. [33,54]. The $\Delta n(T)$ data were then fitted to Eq. (9) (as depicted in Fig. 9), taking the reduced temperature range of $|\tau| = 5 \times 10^{-3}$ with $\Delta = 0.5$ and $D_+ = D_- = 0$. The value of the obtained parameters along with the χ_v^2 value for all the investigated samples is shown in Table IV. It is observed that the value of $C_+ \approx C_- = \Delta n(T_{NA})$ for all the samples, hence suggesting the continuous nature of the second-order N-SmA phase transition [33]. Moreover, the constants A_+ and A_- manifest negative and positive values in the N and SmA regions, correspondingly. The ratio $|A_-/A_+|$ lies within the range of 0.98–1.7, and the maximum value of related χ_v^2 parameter is ~ 1.062. Most importantly, the values of z are consistent with the z' values and vary in a similar fashion to previously obtained α' values for the pure and doped LC samples. As a result, a reasonably good relationship has been established between the values of the critical exponent

TABLE IV. Value of parameters evaluated from the fits of Δn data with Eq. (9) in SmA and N phases and associated χ_v^2 value for the pure 8OCB and QDs doped LC samples. The value of the corrective terms, D_+, D_- is set to zero.

LC sample	Phase	A_+, A_-	C_+, C_-	z, z'	χ_v^2
Pure 8OCB	N	-0.5899 ± 0.3090	0.1529 ± 0.00002	0.2010 ± 0.0516	1.062
	SmA	0.6441 ± 0.2020	0.1526 ± 0.00003	0.2041 ± 0.0301	
$x_{QDs} = 0.1$	N	-0.7096 ± 0.5462	0.1530 ± 0.00005	0.1900 ± 0.0719	1.061
	SmA	0.6995 ± 0.1521	0.1533 ± 0.00001	0.1901 ± 0.0202	
$x_{QDs} = 0.2$	N	-0.5455 ± 0.2910	0.1511 ± 0.00003	0.2070 ± 0.0521	1.062
	SmA	0.6120 ± 0.1015	0.1513 ± 0.00001	0.2072 ± 0.0160	
$x_{QDs} = 0.3$	N	-0.5172 ± 0.2923	0.1546 ± 0.00003	0.2103 ± 0.0551	1.061
	SmA	0.9289 ± 0.3829	0.1547 ± 0.00004	0.2107 ± 0.0402	

TABLE V. Values of the relation $(1-z)$ and parameters (λ and β') evaluated by taking $z \cong z'$, $\lambda = 2\beta$ into consideration for the pure and doped LC samples.

LC sample	$1-z$	$\lambda \ (= 1-\alpha')$	$\beta' \ (= \lambda/2)$
Pure 8OCB	0.7974 ± 0.040	0.7997 ± 0.001	0.3998 ± 0.001
$x_{QDs} = 0.1$	0.8099 ± 0.046	0.8101 ± 0.073	0.4050 ± 0.036
$x_{QDs} = 0.2$	0.7929 ± 0.034	0.7921 ± 0.008	0.3960 ± 0.004
$x_{QDs} = 0.3$	0.7895 ± 0.047	0.7900 ± 0.001	0.3950 ± 0.001

z acquired using this method and α' extracted from both the $Q(T)$ and $E(T)$ fitting functions. Therefore, we can safely consider that $z \cong z'$, and an average value of z is used further to calculate the quantity $1-z$ of the relation $\lambda = 1-z$. Also, it has been discussed earlier that the value of α' evaluated from Eq. (6) for the pure 8OCB LC correlates well with the α critical exponent value. Thus, we assumed the quantity α as α' to compute the value of λ for all the samples, as represented in Table V. The value of λ for the pure 8OCB LC is 0.7997 ± 0.0015, slightly higher than previously reported for the same compound [20]. With the inclusion of QDs as $x_{QDs} = 0.3$, the λ value marginally increases and then decreases with increasing doping concentration in the pure sample, reaching 0.7900 ± 0.0004 for the $x_{QDs} = 0.3$ doped sample. The entire analysis reveals that, for all the studied samples, the equality relation $\lambda = 1-z$ and consequently $\lambda = 1-\alpha$ hold, as predicted by the Landau–de Gennes free energy model. However, for some mesogenic LC compounds, the equality of the relation does not always hold and is found to be $\lambda < 1-\alpha$ based on the N range [43]. As per the scaling theorem for the long-range ordered system, λ is given by $\lambda = 2\beta$, where β is the critical exponent, indicating the limiting behavior of the order parameter at the N-SmA phase transition. It means that the value of λ may fall within the range $2\beta \leqslant \lambda \leqslant 1-\alpha$ for the second-order phase transition.

Generally, the coupling of two different molecular orderings approaches the critical phenomena near the N-SmA phase transition. Originating from the molecular interaction, the effective linkage between the macroscopic N order, S, and the smectic-positional order parameter $|\Psi|$ is reflected by both the N range and fluctuation of the nematic director. Therefore, in another investigation of the critical behavior, we have estimated the coupling strength $\delta(\Delta n)$ via mutual interaction among the host LC molecules and guest NPs. The value of $\delta(\Delta n)$ is calculated by measuring a change in the values of Δn above and below the N-SmA phase transition for all the samples. Since the experimental Δn data exhibit a finite discontinuity followed by a diverging pattern in the vicinity of T_{NA}, a fundamental exponent expression $a + b\,(T_o - T)^c$ is first fitted in the N phase [15] and extrapolated to the SmA region, as indicated in the inset of Fig. 9. Then by keeping the parameters b, T_o, and c fixed, the same equation has been fitted to the data in the SmA phase just below the transition point and extrapolated into the N phase. The obtained difference between the values of a in the N and SmA phases reflects the corresponding $\delta(\Delta n)$ value. Figure 10 depicts the variation of $\delta(\Delta n)$ with the N range for the pure and doped LC systems. A slight decrement is observed in the $\delta(\Delta n)$
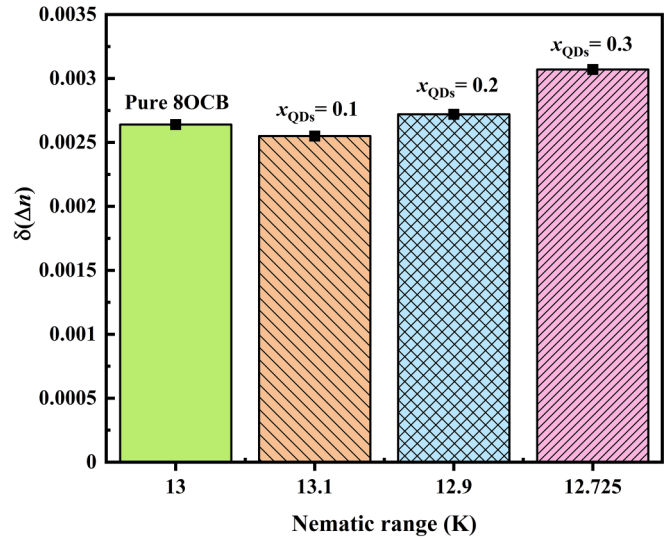
FIG. 10. Variation of the coupling strength $\delta(\Delta n)$ with N range for the pure and doped liquid crystal (LC) samples.

value from 0.0026 in pure to 0.0025 in the $x_{QDs} = 0.1$ doped sample. The coupling between the nematic-orientational and smectic-positional ordering is expected to decrease when the N range increases [19]. Therefore, in the $x_{QDs} = 0.1$ doped sample, the coupling strength decreases slightly because of a small increment in the N range compared with the pure LC due to the mutual interaction between the ligands and mesogenic molecules. At the same time, when the N range decreases, the coupling enhances. Thus, the value of $\delta(\Delta n)$ increases further with increasing doping concentration from 0.1 to 0.2 in the pure sample, and a maximum value is noted for the heavily doped sample as 0.003. Apart from this, it is essential to understand the nature of $\delta(\Delta n)$ through the interaction mechanisms in the doped LC systems. In our earlier investigation [24], we proposed an argument that interaction among ligands of adjacent QDs is also possible, which can affect the orientational ordering of the mesogenic molecules. In the heavily doped samples, the strength of the ligand-ligand interaction is anticipated to be more than in the $x_{QDs} = 0.1$ doped sample. Consequently, this type of ligand interaction disturbs the local ordering of the molecules in the vicinity of nearby QDs, causing a reduction in the N range and enhancement in the coupling between the nematic and smectic order parameters for the $x_{QDs} = 0.2$ and 0.3 doped samples. Therefore, based on the value of $\delta(\Delta n)$ and the nature of the phase transitions as discussed above, we believe that, when the ligand-ligand interaction dominates over the LC-QD ligands interaction, it strengthens the order parameter coupling and causes the transition to move slightly toward the first-order character.

IV. SUMMARY AND CONCLUSIONS

The effect of QD doping on the phase transitional behavior is investigated in detail by utilizing the temperature-dependent high-resolution optical birefringence and dielectric anisotropy data of the pure and QD doped 8OCB LC systems. By investigating the optical birefringence data near the I-N phase

transition, the values of order parameter critical exponent β are found to be consistent with the theoretical hypothesis which describes the weakly first-order character. A dependence of doping concentration on the N-SmA phase transitional nature is studied by fitting the differential forms of optical and dielectric anisotropy data in the vicinity of the transition point. Based on our observations, the evaluated value of heat capacity critical exponent α' for the pure LC agrees well with the values previously reported from the high-resolution ASC and Δn measurements. For the lower doped sample, a slight decrement in the value of α' is observed with a marginal increase in the N range compared with the pure sample. An increment in the doping concentration further increases the α' value by reducing the N range, indicating an enhancement in the coupling strength between the N and SmA order parameters. The effectiveness of the estimated α' values has been verified with the aid of the χ_v^2 profile minima. Moreover, good consistency is achieved between the α' values extracted from both the optical birefringence and dielectric anisotropy measurements. The McMillan ratio R_M appeared to be ~ 0.963 for the $0 \leqslant x_{QDs} \leqslant 0.3$ LC compounds and outline the second-order character of the N-SmA phase transition, which is not much affected by the presence of QDs in the LC matrix. A scaling relation with α' is also found to be validated using the experimentally obtained values. Furthermore, the coupling efficiency between the N and SmA order

parameters shows a slight reduction in the $x_{QDs} = 0.1$ doped sample and then increases monotonically as the doping concentration increases. The ligand-ligand interaction predominates in the $x_{QDs} = 0.2$ and 0.3 doped samples, which enhanced the coupling strength among the order parameters by decreasing the N range. Hence, the overall obtained results indicate that the LC-QDs ligand interaction plays an important role in influencing the N-SmA phase transitional behavior. It can be stated that there is a slight tendency for the phase transition to approach the first-order character due to the strong coupling between orientational and translational ordering. However, a deeper insight into the interaction mechanisms by varying the size and shape of differing NPs will further help to understand the correlation between the coupling strength and associated effect on phase transitional behavior from the perspective of both experimental and theoretical works.

[1] J. P. F. Lagerwall and G. Scalia, Curr. Appl. Phys. **12**, 1387 (2012).

[2] J. Tang, F. Liu, M. Lu, and D. Zhao, Sci. Rep. **10**, 18067 (2020).

[3] A. Choudhary, T. F. George, and G. Li, Biosensors **8**, 69 (2018).

[4] S. Özğan, H. Eskalen, and Y. Tapkiranli, J. Mater. Sci.: Mater. Electron. **33**, 5720 (2022), and references therein.

[5] R. Basu and G. S. Iannacchione, Phys. Rev. E **81**, 051705 (2010).

[6] R. K. Shukla, A. Chaudhary, A. Bubnov, V. Hamplova, and K. K. Raina, Liq. Cryst. **47**, 1379 (2020).

[7] R. K. Shukla, K. K. Raina, V. Hamplova, M. Kaspar, and A. Bubnov, Phase Transit. **84**, 850 (2011).

[8] R. K. Shukla, A. Chaudhary, A. Bubnov, and K. K. Raina, Liq. Cryst. **45**, 1672 (2018).

[9] P. Kalakonda and G. S. Iannacchoine, Phase Transit. **88**, 547 (2015).

[10] M. Gorkunov and M. Osipov, Soft Matter **7**, 4348 (2011).

[11] J. Łoś, A. Drozd-Rzoska, S. J. Rzoska, and K. Czupryński, Eur. Phys. J. E **45**, 74 (2022).

[12] S. J. Rzoska, S. Starzonek, J. Łoś, A. Drozd-Rzoska, and S. Kralj, Nanomaterials **10**, 2343 (2020).

[13] K. J. Stine and C. W. Garland, Phys. Rev. A **39**, 3148 (1989).

[14] B. Rožič, E. Karataira, G. Nounesis, V. Tzitzios, G. Cordoyiannis, S. Kralj, and Z. Kutnjak, Mol. Cryst. Liq. Cryst. **553**, 161 (2012).

[15] A. Mertelj, L. Cmok, M. Čopič, G. Cook, and D. R. Evans, Phys. Rev. E **85**, 021705 (2012).

[16] S. J. Rzoska, S. Starzonek, A. Drozd-Rzoska, K. Czupryński, K. Chmiel, G. Gaura, A. Michulec, B. Szczypek, and W. Walas, Phys. Rev. E **93**, 020701(R) (2016).

[17] M. K. Das, P. C. Barman, and S. K. Sarkar, Eur. Phys. J. B **88**, 175 (2015).

[18] K. P. Sigdel and G. S. Iannacchione, Eur. Phys. J. E **34**, 34 (2011).

[19] S. Yildiz, M. C. Cetinkaya, and H. Ozbek, Fluid Ph. Equilibria **495**, 47 (2019).

[20] A. Chakraborty, S. Chakraborty, and M. K. Das, Phys. Rev. E **91**, 032503 (2015).

[21] G. Cordoyiannis, C. S. P. Tripathi, C. Glorieux, and J. Thoen, Phys. Rev. E **82**, 031707 (2010), and references therein.

[22] S. Chakraborty, A. Chakraborty, M. K. Das, and W. Weissflog, Phase Transit. **92**, 806 (2019).

[23] S. Chakraborty, A. Chakraborty, M. K. Das, and W. Weissflog, J. Mol. Liq. **219**, 608, (2016).

[24] A. Rani, S. Chakraborty, and A. Sinha, J. Mol. Liq. **342**, 117327 (2021).

[25] S. Patranabish, Y. Wang, A. Sinha, and A. Majumdar, Phys. Rev. E **103**, 052703 (2021).

[26] P.-C. Wu and W. Lee, Appl. Phys. Lett. **102**, 162904 (2013).

[27] Y. Lin, A. Daoudi, F. Dubois, J.-F. Blach, J.-F. Henninot, O. Kurochkin, A. Grabar, A. Segovia-Mera, C. Legrand, and R. Douali, RSC Adv. **7**, 35438 (2017).

[28] H. Ayeb, S. Alaya, M. Derbali, L. Samet, J. Bennaceur, F. Jomni, and T. Soltani, Liq. Cryst. **48**, 223 (2021).

[29] M. V. Rasna, L. Cmok, D. R. Evans, A. Mertelj, and S. Dhara, Liq. Cryst. **42**, 1059 (2015).

[30] H. Atkuri, G. Cook, D. R. Evans, C.-I. Cheon, A. Glushchenko, V. Reshetnyak, Y. Reznikov, J. West, and K. Zhang, J. Opt. A: Pure Appl. Opt. **11**, 024006 (2009).

[31] M. F. Vuks, Opt. Spectrosc. **20**, 361 (1966).

[32] S. Chandrasekhar and N. V. Madhsudana, J. Phys. (Paris) Colloq. **30**, C4 (1969).

[33] S. Erkan, M. Çetinkaya, S. Yildiz, and H. Ozbek, Phys. Rev. E **86**, 041705 (2012).

[34] M. C. Cetinkaya, S. Ustunel, H. Ozbek, S. Yildiz, and J. Thoen, Eur. Phys. J. E **41**, 129 (2018), and references therein.

[35] P. R. Bevington and D. K. Robinson, *Data Reduction and Error Analysis for the Physical Sciences*, 3rd ed. (Mc Graw Hill, New York, 2003).

[36] P. H. Keyes, Phys. Lett. A **67**, 132 (1978).

[37] M. A. Anisimov, S. R. Garber, V. S. Esipov, V. M. Mamnitskii, G. I. Ovodov, L. A. Smolenko, and E. L. Sorkin, Sov. Phys. JETP **45**, 1042 (1977).

[38] M. A. Anisimov, Mol. Cryst. Liq. Cryst. **162**, 1 (1988).

[39] S. Yildiz, M. C. Cetinkaya, H. Ozbek, V. Tzitzios, and G. Nounesis, J. Mol. Liq. **298**, 112029 (2020).

[40] P. G. de Gennes, Mol. Cryst. Liq. Cryst. **21**, 49 (1973).

[41] K.-C. Lim and J. T. Ho, Phys. Rev. Lett. **40**, 944 (1978).

[42] M. E. Fisher and A. Aherony, Phys. Rev. Lett. **31**, 1238 (1973).

[43] K. K. Chan, M. Deutsch, B. M. Ocko, P. S. Pershan, and L. B. Sorensen, Phys. Rev. Lett. **54**, 920 (1985).

[44] P. G. de Gennes and J. Prost, *The Physics of Liquid Crystals*, 2nd ed. (Oxford University Press, Oxford, 1993).

[45] M. Marinelli, F. Mercuri, and U. Zammit, in *Heat Capacities: Liquids, Solutions, and Vapours*, edited by E. Wilhelm and T. M. Letcher (Royal Society of Chemistry, London, 2010).

[46] S. Yıldız, M. C. Çetinkaya, Ş. Ustünel, H. Ozbek, and J. Thoen, Phys. Rev. E **93**, 062706 (2016), and references therein.

[47] F. Cruceanu, D. Liang, R. L. Leheny, C. W. Garland, and G. S. Iannacchione, Phys. Rev. E **79**, 011710 (2009).

[48] A. V. Kityk and P. Huber, Appl. Phys. Lett. **97**, 153124 (2010).

[49] H. E. Stanley, *Introduction to Phase Transitions and Critical Phenomena* (Oxford University Press, New York, 1971).

[50] J. Thoen, H. Marynissen, and W. Van Dael, Phys. Rev. A **26**, 2886 (1982).

[51] M. C. Çetinkaya, S. Yildiz, H. Ozbek, P. Losada-Pérez, J. Leys, and J. Thoen, Phys. Rev. E **88**, 042502 (2013).

[52] C. W. Garland, in *Liquid Crystals: Experimental Study of Physical Properties and Phase Transitions*, edited by S. Kumar (Cambridge University Press, Cambridge, 2001).

[53] C. W. Garland and G. Nounesis, Phys. Rev. E **49**, 2964 (1994).

[54] A. Zywociński, S. A. Wieczorek, and J. Stecki, Phys. Rev. A **36**, 1901 (1987).

[55] P. Cusmin, M. R. de la Fuente, J. Salud, M. A. Pérez-Jubindo, S. Diez-Berart, and D. O. López, J. Phys. Chem. B **111**, 8974 (2007).

[56] J. Łoś, A. Drozd-Rzoska, S. J. Rzoska, S. Starzoneka, and K. Czupryński, Soft Matter **18**, 4502 (2022).

[57] J. Łoś, A. Drozd-Rzoska, and S. J. Rzoska, J. Mol. Liq. **377**, 121555 (2023).